International Journal of Environmental Sciences
ISSN: 2229-7359
Vol. 11 No. 23s, 2025
https://theaspd.com/index.php

Implementation of Neural Network-Based Control System for MT-Upqc$_{\mu g}$ to Enhance Power Quality

Manjula M G[1], Dr. Surendra S[2], Dr. Veeresha K B[3]
[1]Asst. Professor, Dept. of EEE, JNNCE, Shimoga, Karnataka, India
[2]Head and Professor, Dept. of ETE, JNNCE, Shimoga, Karnataka, India
[3]Asst. Professor, Dept. of EEE, JNNCE, Shimoga, Karnataka, India

Abstract: *The integration of distributed generation and renewable energy sources in Microgrids introduces significant challenges in maintaining Electrical Power Quality (EPQ) and ensuring system stability. This paper addresses the mitigation of EPQ issues, such as voltage sags, swells, and harmonics, by incorporating a Multi-Terminal Unified Power Quality Conditioner (MT-UPQC) into a hybrid photovoltaic–wind–battery Microgrid system. The effectiveness of the PV-wind-battery-UPQC system is demonstrated through MATLAB/Simulink simulations. In this setup, the shunt controllers leverage the PQ theory, whereas the series controller utilizes the Unit Vector Template approach. Results reveal notable enhancements in power quality, characterized by substantial reductions in harmonic distortions and voltage fluctuations compared to conventional techniques. Moreover, the implementation of an Artificial Neural Network (ANN)-based control strategy enhances system stability across diverse operating conditions, thereby providing a dependable solution for maintaining superior power quality within complex microgrid environments. Nonlinear, unbalanced loads and harmonic supply voltages are used to assess the performance of the Renewable energy systems combining solar PV, wind power, and battery storage with grid integration, which is controlled by an artificial neural network. MATLAB/Simulink simulations demonstrate the efficacy of integrating PV, wind, and battery systems with a Unified Power Quality Conditioner (UPQC). The control strategy involves PQ theory for shunt controllers and Unit Vector Template Generation for series controllers. This approach yields substantial power quality enhancements, minimizing harmonic distortions and voltage instability issues. Moreover, Artificial Neural Network (ANN) control enhances system resilience and adaptability, ensuring reliable operation across diverse microgrid scenarios.*
Index Terms: *Microgrid, Distributed Generation (DG), Power Quality (PQ), THD (Total Harmonic Distortion), UPQC (Unified Power Quality Conditioners).*

1. INTRODUCTION:

Both solar and wind energy are renewable and environmentally friendly energy sources. Despite the advantages of solar energy, photovoltaic (PV) systems often struggle with the dynamic and nonlinear characteristics of solar radiation which can reduce energy harvesting to suboptimal levels. Wind energy faces its own challenges as wind speeds are often inconsistent, making it difficult to capture energy reliably. Compared to traditional methods, the application of artificial intelligence (AI) in energy harvesting has the potential to bring major improvements in effectiveness, productivity, and innovation. An example of this is the work of Saude who designed a microgrid powered by solar and wind energy for use on the Moon and Mars [1]. Other studies have also demonstrated the implementation of PV-wind-battery systems with multimodal control methods for grid-side converters [2].

The use of a bidirectional converter for power flow control in a microgrid is discussed in [3], including considerations of the battery's state of charge (SOC). Furthermore, a Microgrid system with an LCL filter was developed and connected to the grid using a firefly algorithm [4]; also, a PV-wind-battery Microgrid system was studied [5]. In reference [6], multilevel converters with shared DC bus and DDPMSG together with solar array and battery energy control system (BECS) are presented. An implementation of an ideal system using combined wind, solar and grid electricity can be found in [7].

The UPQC FLC EVA approach has been utilized to improve power and grid stability in renewable energy systems [8], and inverter strategies for grid-connected PV systems have been described [9]. Another research analysed and improved a PV system with a bidirectional LLC converter [10] and the design and modelling of an energy management system was introduced [11].

A feed forward neural network, trained using particle swarm optimization (PSO), was applied to PV arrays [12], and the Levenberg–Marquardt (LM), Bayesian Regularization (BR), and Scaled Conjugate Gradient (SCG) algorithms were employed on PV systems with ANN [13]. Wind energy integrated with ANN offered insights into the superiority of the LM algorithm, though these studies did not consider battery integration [14]. Other research on PV–wind–battery–grid systems involving permanent magnet synchronous generators (PMSGs) and lead-acid batteries has mainly focused on bidirectional converters, with limited use of AI techniques [15]. Some authors [16] suggested using AI controllers for future Renewable energy systems combining solar PV, wind power, and battery storage with grid integration systems with doubly fed induction generators (DFIG), while others have focused on specific performance improvements. Hybrid systems without wind integration remain an area of research [17].

The present research on renewable energy systems identifies many significant difficulties that must be solved. Deficient approaches to grid synchronization have been discussed in the literature [18], insular range of testing scenarios which do not consider many external factors [19], incomplete system integration processes [20], insufficiently developed optimization methods [21], concerns regarding the scalability of these methods [22], and insufficient robustness explained in the literature [23]. Addressing these gaps poses an opportunity for rigorous research to enhance the effectiveness, efficiency, and adaptability of renewable energy systems.

The proposed system builds on previous work by combining solar PV, wind power, and battery storage with grid architecture that uses a permanent magnet synchronous generator (PMSG) alternator and a lithium-ion battery. It also uses an artificial neural network (ANN) that has been optimized with the Levenberg–Marquardt (LM) algorithm [24]. It has an LCL filter and a bidirectional converter, among other things, that let you control both current and voltage [25]. This model uses a control method that is more flexible than those used in previous studies. The LM algorithm has been shown to work well for controlling either PV or wind systems on their own in earlier studies [26] [27]. However, the proposed method combines both systems for complete power flow management [28].

A more sophisticated and all-encompassing strategy is achieved by including current and voltage management in addition to specialized parts like the LCL filter and inverter control. In order to integrate renewable energy into microgrids, the "Introduction" section discusses a number of renewable energy systems that combine solar PV, wind power, and battery storage with grid integration systems and ANN controllers. The 3T-UPQCμG's simulation model, operating modes, and schematic diagram are covered in the "3T-UPQCμG configuration" section. The "Mathematical Modelling" section discusses the ANN controller and mathematical models for the PV, wind turbine, PMSG, and battery systems. The "Levenberg-Marquardt algorithm" describes the step by step procedure of algorithm to this model. The "Analysis and Design of Controllers" section explains the implementation of the LM algorithm in the ANN controller, the training process, mean squared error (MSE), and error histogram with performance metrics. The "Simulation Results" section presents the simulation results harmonics, voltage sag, voltage swell, grid and islanding modes with power waveforms. Finally, the "Conclusion" section summarizes the findings of the study.

2. 3T-UPQC$_{\mu G}$ CONFIGURATION:

The incorporation of the 3T-UPQC, which has two shunt active filters and one series, into a utility-connected Microgrid

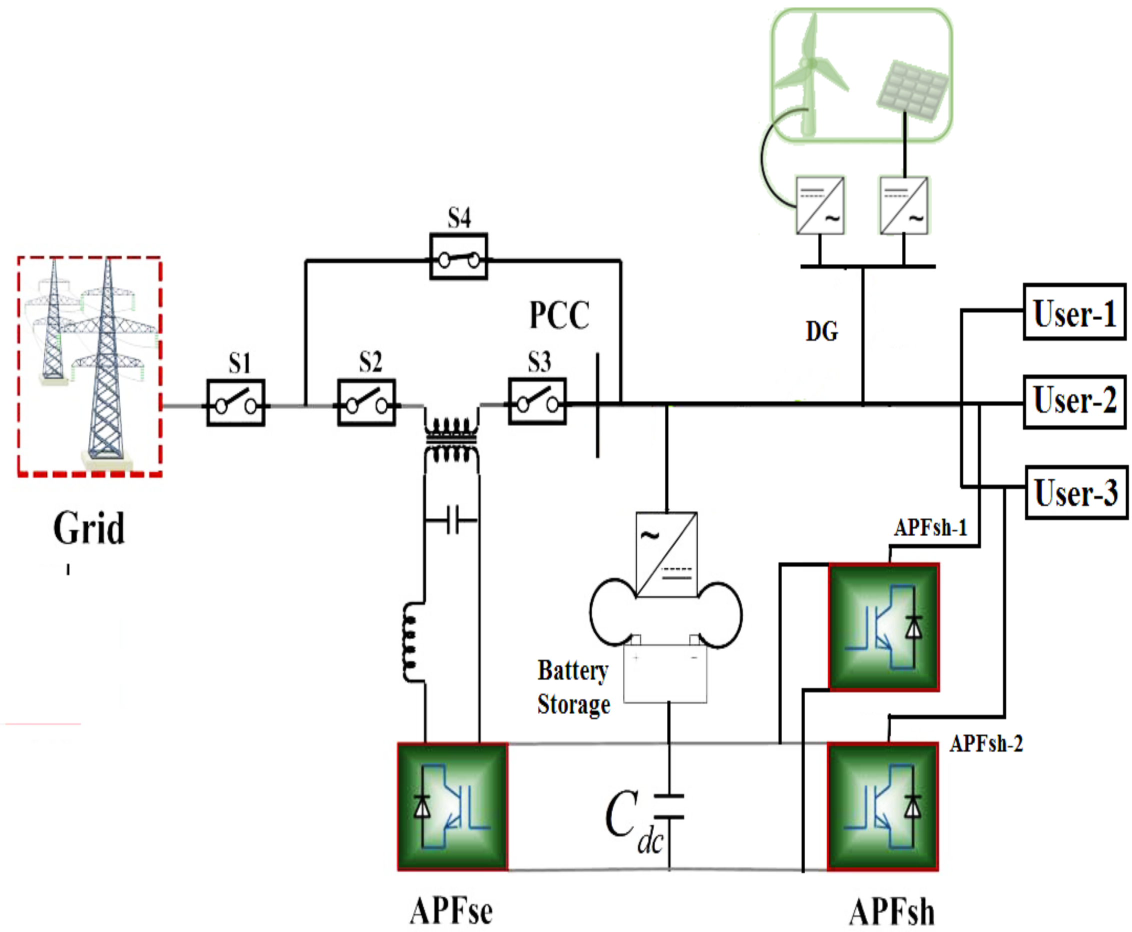

system is illustrated in Figure 1 [22]. Its primary function is to operate in two modes.

Figure 1: Schematic diagram of the 3T-UPQCμG

The proposed 3T-UPQC$_{\mu G}$ has two basic operating modes.

▪ **Interconnected mode**

- The DG source provides the actual power to the load and storage. The grid's basic active power is also supplied by the DG source.
- The series portion of UPQC (APF$_{se}$) compensates for voltage sag, flickers, voltage swell, and transients by transmitting active power from storage or the grid.
- The shunt portion of the UPQC (APF$_{sh}$) compensates for the reactive power of the non-linear load and eliminates harmonic distortions to maintain the THD within the bounds.
- The UPQC delivers a signal to a small Microgrid system with distributed generations to respond to an emergency (blackout) caused by a sudden interruption or breakdown.

▪ **Islanded mode**

- When the grid fails, the series section of the UPQC is disconnected, while the DG converter balances the voltage at the PCC level.
- To ensure smooth current at the PCC, the nonlinear load reactive component is compensated by the shunt part of the UPQC while remaining connected.
- The DG converter delivers only active power with storage. It isn't unplugged from the system.
- When grid power is restored, the UPQC series is reconnected.

▪ **Simulations Model**

A 3-phase, 3-wire active distribution system (400VL-N) featuring the suggested UPQC$_{\mu G}$ and μG, illustrated in Figure 2, has been created within the MATLAB environment. Details of the performance with the simulation results in grid-connected and Island mode are given below.

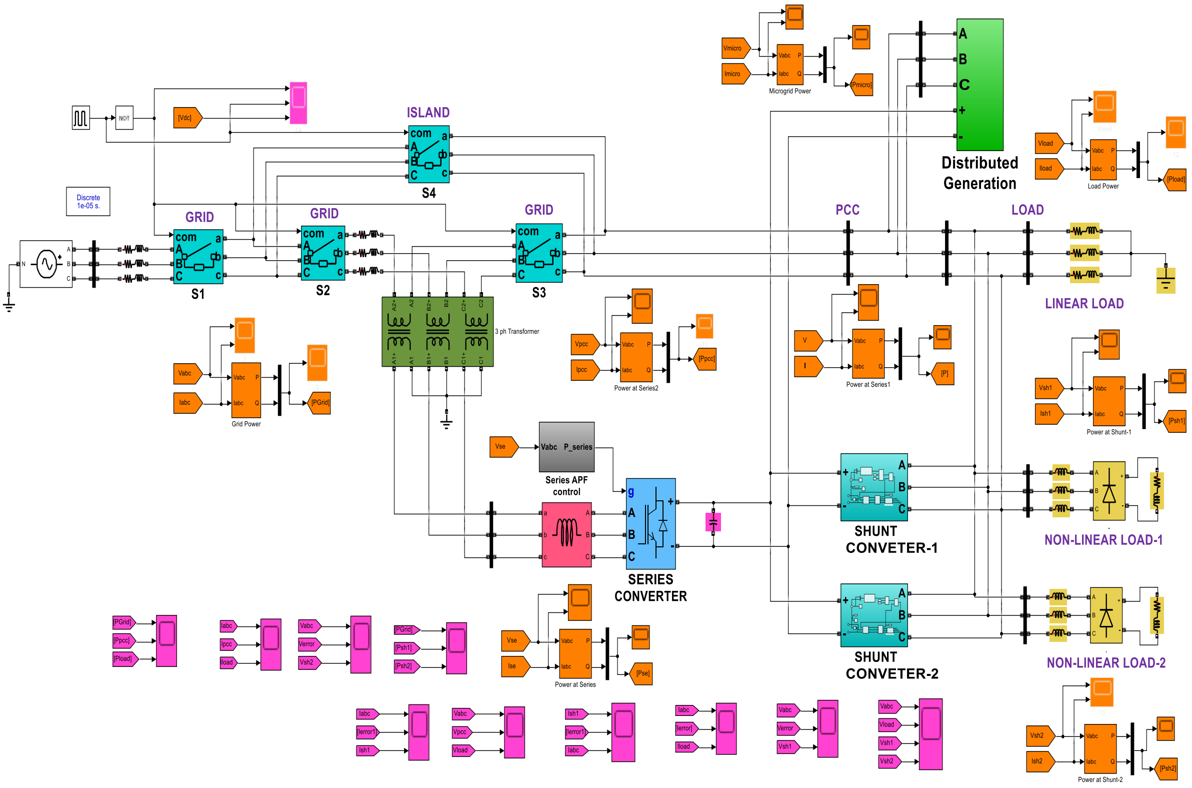

Figure 2: Micro-grid with three terminal UPQC

3. Mathematical Modelling:

Photovoltaic system:

This analysis calculates the temperature of photovoltaic cells under changing irradiance and ambient temperature conditions.

$$\mathbf{I = I_{ph} - I_0 \left[e^{\frac{q(v+IR_s)}{\propto KTN_s}} \right] - \left(\frac{V+IR_s}{R_{sh}} \right)} \qquad (1)$$

In this context, I_o, I_{ph} and I represent the current of the diode saturation current, photon current, and PV panel, in that order. R_{sh} and R_s denote the shunt resistance and series resistance, with the shunt resistance in parallel with the forward-biased diode

$$\mathbf{I_d = I_0 \left[e^{(V_d/V_T)} - 1 \right]} \qquad (2)$$

$$\mathbf{I_0 = I_n \left({T_n}/{T} \right) e^{\left[\frac{qE_g}{aK} \left(\frac{1}{T_n} - \frac{1}{T} \right) \right]}} \qquad (3)$$

The parameters I_{SCS}, I_{MPS}, V_{OCs}, and V_{MPS} are stated. TC is the cell temperature.

$$\mathbf{T_c = (T_{Noct} - T_{aNoct}) + \frac{G_t}{G_{tNoct}} \left(1 - \frac{\eta_e}{T_\alpha} \right) + T_a + k\omega_r} \qquad (4)$$

$$\mathbf{\eta_e = \eta_R [1\text{-}\beta(T_{Noct} - T_{aNoct})]} \qquad (5)$$

Equation (6) describes the photon current, Iph

$$\mathbf{I_{ph} = (I_{sc} + \alpha\, \Delta T) \frac{G}{G_{STC}}} \qquad (6)$$

$$\mathbf{I_{sc}\,(G, T_c) = I_{scs} \frac{G}{G_{STC}} [1 + \alpha\, (T_c - T_s)]} \qquad (7)$$

$$\mathbf{V_{oc}\,(T_c) = V_{ocs} + \beta(T_c - T_s)} \qquad (8)$$

Based on the gathering of irradiance and temperature data, irradiance is computed as G (W/m2) [13];

$$\mathbf{G = [(G_{max} - G_{min}) \times rand] + G_{min}} \qquad (9)$$

Temperature T (°C):

$$\mathbf{T = [(T_{max} - T_{min}) \times rand] + T_{min}} \qquad (10)$$

Maximum Voltage, I_{MP} (V):

$$\mathbf{I_{MP}\,(G, T_c) = I_{MPS} \frac{G}{G_{STC}} [1 + \alpha\, (T_c - T_s)]} \qquad (11)$$

Maximum Voltage, V_{MP} (V):

$$\mathbf{V_{MP}\,(T_c) = V_{MPS} + \beta(T_c - T_s)} \qquad (12)$$

Maximum Power,

P_{MP} (W): $\mathbf{P_{MP} = V_{MP} \times I_{MP}}$ (13)

Wind Turbine Aerodynamic:

The power coefficient Cp is calculated using the following equations.

$$\mathbf{C_p(\lambda,\beta) = C_1\left(\frac{C_2}{\lambda_i} - C_3\,\beta - C_4\right)e^{\frac{-c_5}{\lambda_i}} + c_6\lambda} \qquad (14)$$

Where, ρ represents air density and β denotes the wind turbine's blade pitch angle

$$\mathbf{Pm = \frac{1}{2}\rho A C_p(\lambda,\beta) v_w^3} \qquad (15)$$

Battery Energy System:

The battery parameters SOC_0 (initial state of charge), Q_N (nominal capacity), and i_{BAT} (battery current) are calculated for normal battery operation. The current is considered positive during discharge and negative during charge, with 'it' representing the time of battery operation.

$$\mathbf{SOC = SOC_0 - \frac{1}{Q_N}\int_0^t i_{Ba}\,dt = SOC_0 - \frac{it}{Q_N}\,;\ it = \int_0^t i_{Ba}\,dt} \qquad (16)$$

4. Levenberg-Marquardt (LM) algorithm:

The LM algorithm is a powerful and efficient optimization method often used for training Artificial Neural Networks (ANNs), especially in regression problems and function approximation tasks. Here's a step-by-step procedure of this algorithm.

Step 1: Initialize Parameters
1. Provide an initial guess for the model parameters.
2. Set the damping factor (λ) and other hyper parameters.

Step 2: Compute the Residuals
1. Calculate the residuals between observed data and predicted values.
2. Compute the sum of the squared residuals (χ^2).

Step 3: Jacobian Matrix Calculation
1. Calculate the Jacobian matrix (J) of the residuals with respect to the parameters.

Step 4: Update Parameters
1. Compute the update direction using the Levenberg-Marquardt update rule.
2. Update the parameters using the computed direction.

Step 5: Check Convergence
1. Evaluate the new residuals and χ^2.
2. Check if the parameters have converged or the maximum number of iterations is reached.

Step 6: Adjust Damping Factor
1. If the update improves the fit, decrease λ.
2. If the update worsens the fit, increase λ and retry.

Step 7: Repeat Steps 2-6
1. Continue iterating until convergence or maximum iterations.

The Levenberg-Marquardt algorithm iteratively refines the parameters to minimize the sum of squared residuals, providing a robust and efficient solution for non-linear least squares problems.

5. Analysis and Design of Controllers:

The LM algorithm was implemented in an ANN-based controller. At 624 epochs, a photovoltaic gradient value of 0.000000394 was achieved, demonstrating an improvement over the prior outcomes [13, 17]. As shown in Figure 3b, the gradient further reduced to 0.0000003354 at 624 epochs, indicating only a minor deviation in the training data [5]. In Figure 3a, the regression value is 1, reflecting a perfect correlation between predicted and actual outputs. The validation dataset shows a very low error rate of 0.000021, as seen in the error histogram (Figure 3d).

International Journal of Environmental Sciences
ISSN: 2229-7359
Vol. 11 No. 23s, 2025
https://theaspd.com/index.php

The implementation of the LM-based MPPT controller is validated by these minimal gradient and momentum values (Figure 3b). The vertical bars in Figure 3d represent the distribution of errors across the dataset. In a NN, the activation function determines whether a neuron should transmit a signal. It enables the network to learn complex, nonlinear patterns. Without it, the network would behave like a linear model, regardless of how many layers it has. The aggregation function, on the other hand, defines how a neuron combines its inputs usually by summing them before the result is passed through the activation function.

Historical data on wind speed, air density, and direction were used to train the ANN. For wind speed prediction, the ANN controller delivered accurate results across multiple tests, enabling the optimization of wind turbine operations. The best validation performance was achieved at 545 epochs, with a remarkably low error of 0.0000131, as illustrated in Figure 3f. The validation dataset error is 0.001031, observed in the center of the histogram in Figure 3h. Overall, the application of the LM algorithm to the ANN controller led to a noticeable improvement in energy efficiency and a reduction in system stress and operational fluctuations, even under dynamic ambient conditions.

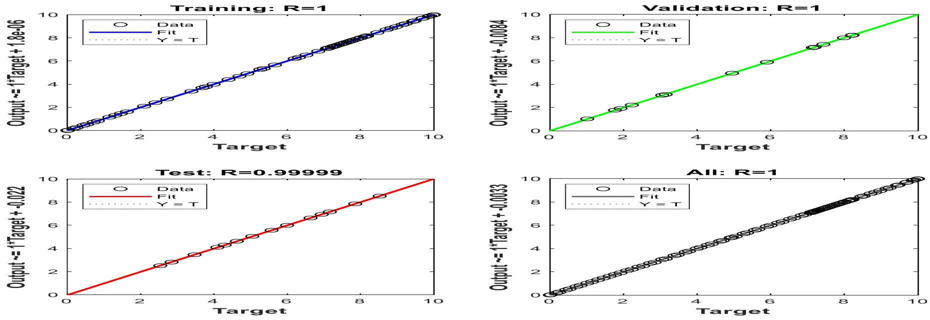

Figure-3a: Regression plot of PV

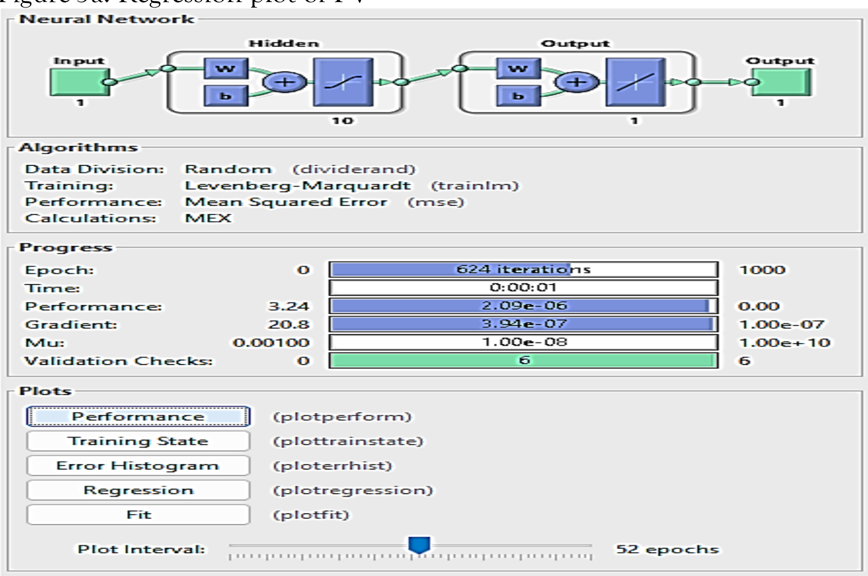

Figure-3b: Neural Network training data for PV

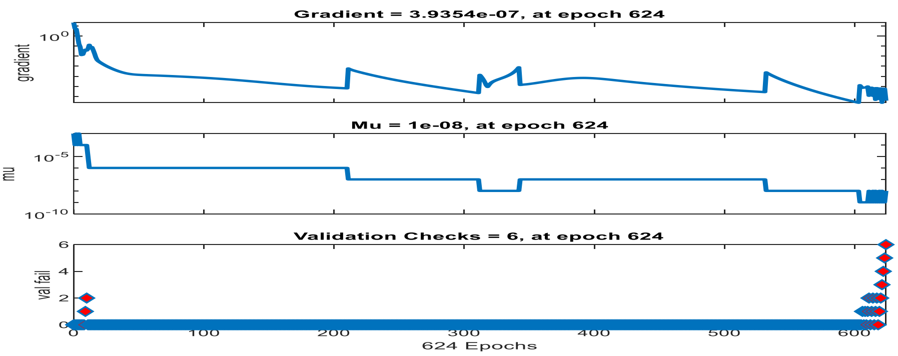

Figure-3c: Training state of PV

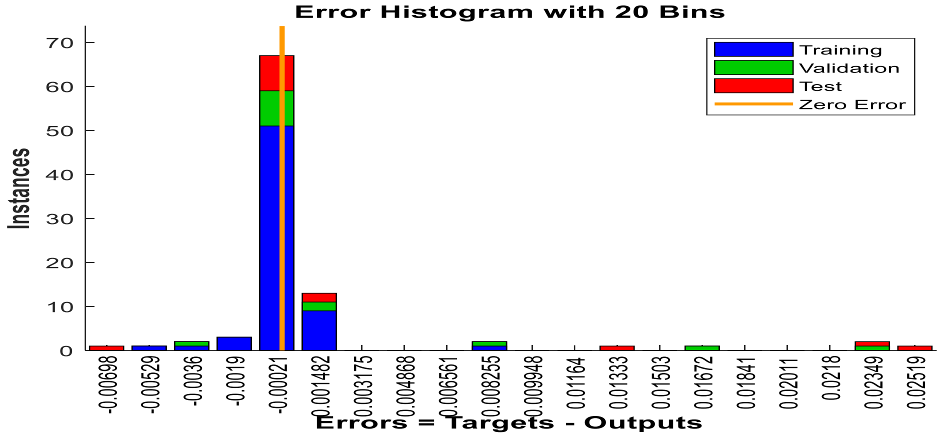

Figure-3d: Error histogram plot of ANN controller PV

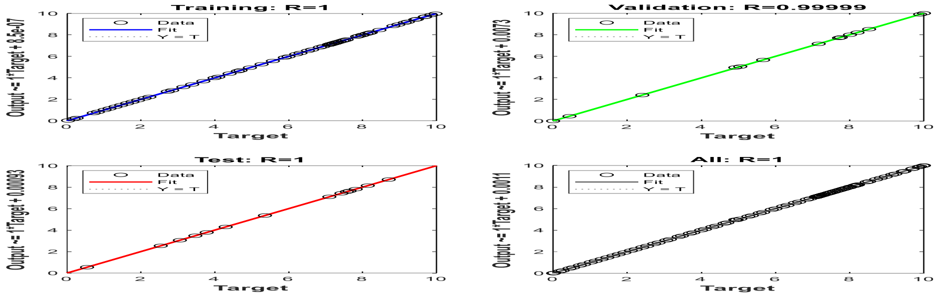

Figure-3e: Regression plot of wind

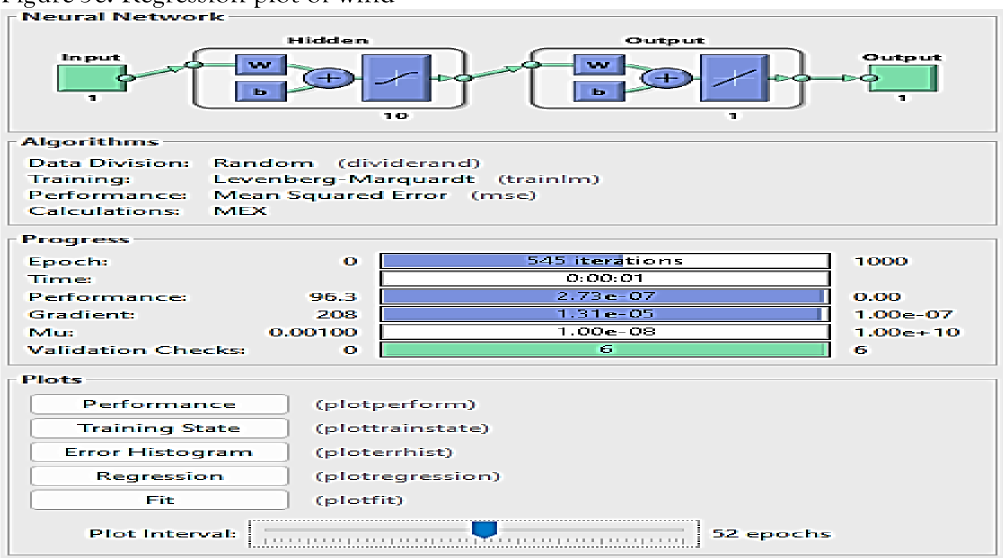

Figure-3f: Neural Network training data for wind

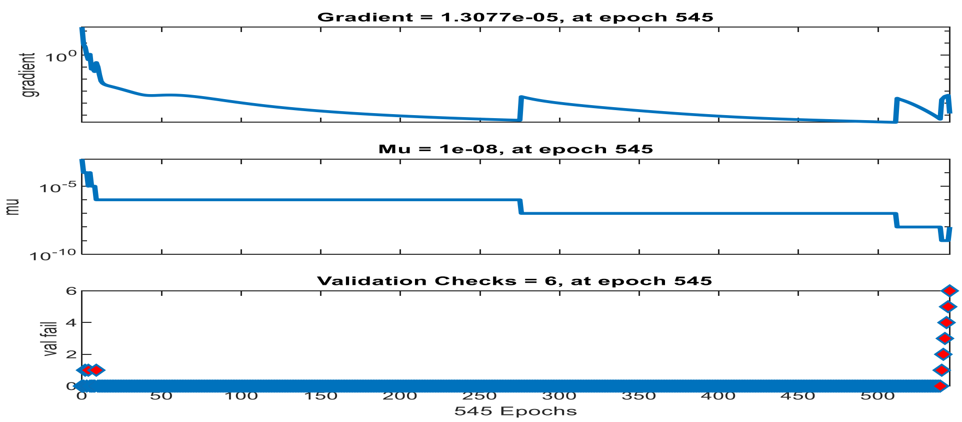

Figure-3g: Training state of wind

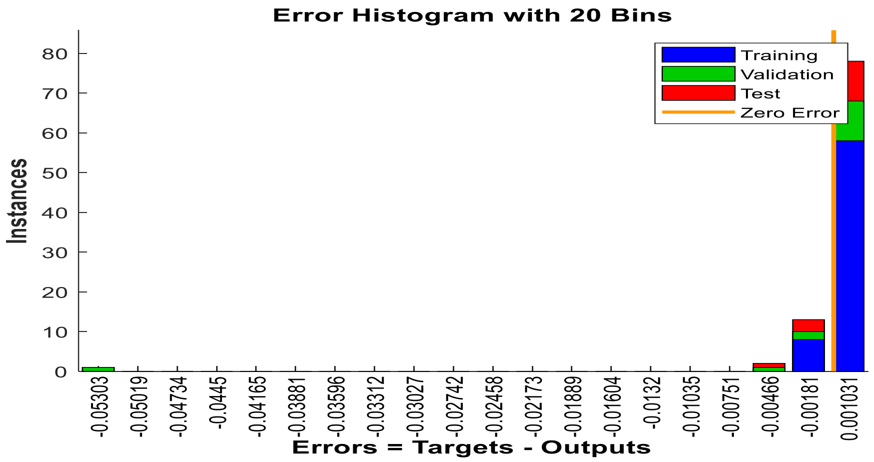

Figure-3h: Error histogram plot of ANN controller**6. Simulation parameters:**

In order perform the simulation study of 3T-UPQCμG following parameters are taken for PV, wind, battery, LCL filter and for inverter.

Table 1: Photovoltaic panel and array specifications

Sl. No.	**Solar PV panel** (Kyocera KD135GX-LPU)	**Module data**
a.	Maximum Power	135
b.	Number of Cells per Panel	50
c.	Open-Circuit Voltage $\mathbf{V}_{oc}$	22 V
d.	Short-Circuit Current $\mathbf{I}_{sc}$	8.3695 A
e.	Maximum Power Point Current $\mathbf{I}_{MP}$	7.6296 A
f.	Maximum Power Point Voltage $\mathbf{V}_{MP}$	17.7 V
g.	Temperature coefficient of $\mathbf{I}_{sc}$	5.02 x 10-3 A/°C
h.	Temperature coefficient of $\mathbf{V}_{oc}$	-8.0 x 10-2 V/°C
i.	Light-Generated Current $\mathbf{I}_{L}$	8.3695 A
j.	Diode Saturation Current $\mathbf{I}_{0}$	4.1601×10^{-10} A
k.	Diode Ideality Factor	1.019
l.	R_{sh}	224.188 Ω
m.	R_{s}	0.23724 Ω

Table 2: PV array configuration

Sl. No	**PV Array**	**data**
a.	Number of Parallel strings	15
b.	String in each Modules	5
c.	Number of cells per module	36

Table 3: Battery Specifications

Sl. No.	Parameter	Value
a.	Capacity	48 Ah
b.	Voltage cut-off	180 V
c.	Fully charged voltage	279.35 V
d.	Discharge current	20.86 A
e.	Resistance Internal	0.5 Ω
f.	Capacity voltage	43.40 V
g.	Voltage nominal	240 V

Table 4: Wind Turbine Parameters

Sl. No.	Parameter	Rating
a.	Capacity	10 kW
b.	Wind speed	12 m/s
c.	Minimum wind speed	3 m/s
d.	Maximum wind speed	25 m/s
e.	Rotor Diameter	5 m

Table 5: LCL Filter and Inverter Parameters

Sl. No.	Parameter	Rating
a.	DC bus voltage	800 V
b.	Grid voltage	400 V
c.	Grid frequency	50 Hz
d.	Switching frequency	10 kHz
e.	Rated Power	10 KVA
f.	Inductor Lin	4.06 mH
g.	Inductor Lg	4.35 mH
h.	Capacitor	6666 uF
i.	Controller time constant	150 us
j.	Proportional Gain, Kp	27.066
k.	Resonant Gain, Kr	100

7. Simulation results:

a. Harmonics compensation by Shunt converter for load current

Shunt converters are employed to mitigate current harmonics generated by nonlinear loads. Initially, the source and load currents have similar waveforms. The Total Harmonic Distortion (THD) of the source current before compensation is approximately 24.99% (Figure 4a) for Nonlinear Load-1 and 29.31% (Figure 6a) for Nonlinear Load-2.

However, with the introduction of Shunt converter-1 at non-linear load-1, it injects the necessary current component to render the source current virtually harmonic-free, as depicted in Figure 3. Consequently, the source current becomes almost sinusoidal after compensation. The THD of the source current decreases significantly to 4.37%, as shown in Figure 4b with PI control`ler and 0% with ANN controller as shown in figure 4c.

Similarly, with respect to non-linear load-2, Shunt converter-2 (figure 5) reduce the THD from 29.21% (figures 6a) to 4.37% (figures 6b) with PI controller and 0% (figures 6c) with ANN controller. Table 1 summarizes the THD values before and after DSTATCOM compensation.

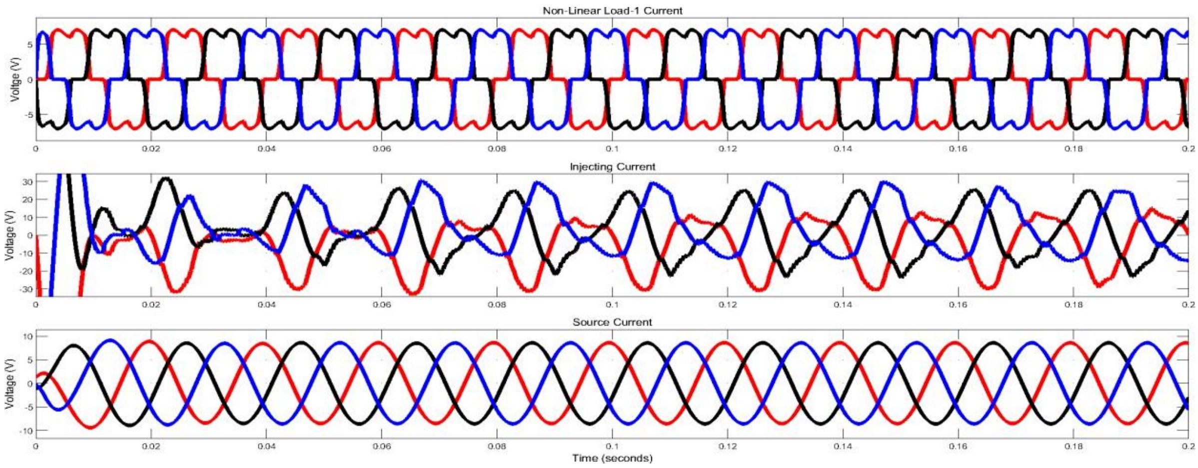

Figure 3: Non-linear load-1, Injecting and Source currents

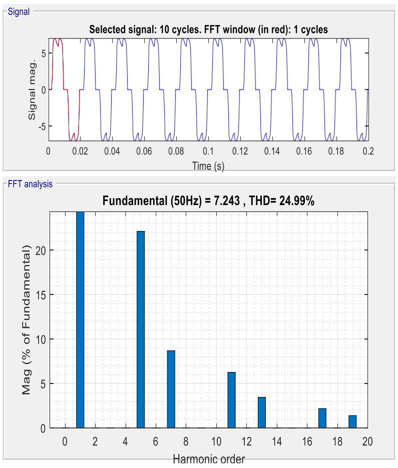

Figure 4a: Load current

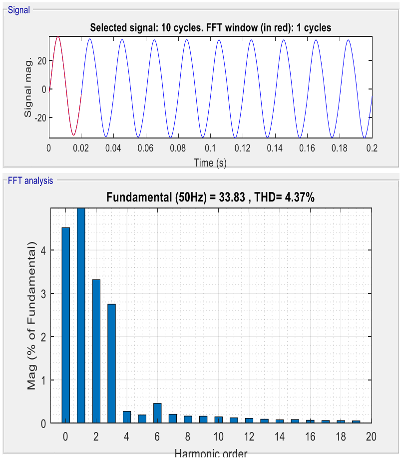

Figure 4b: Source current (PI)

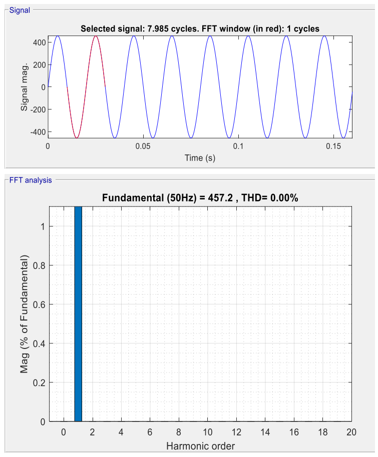

Figure 4c: Source current (ANN)

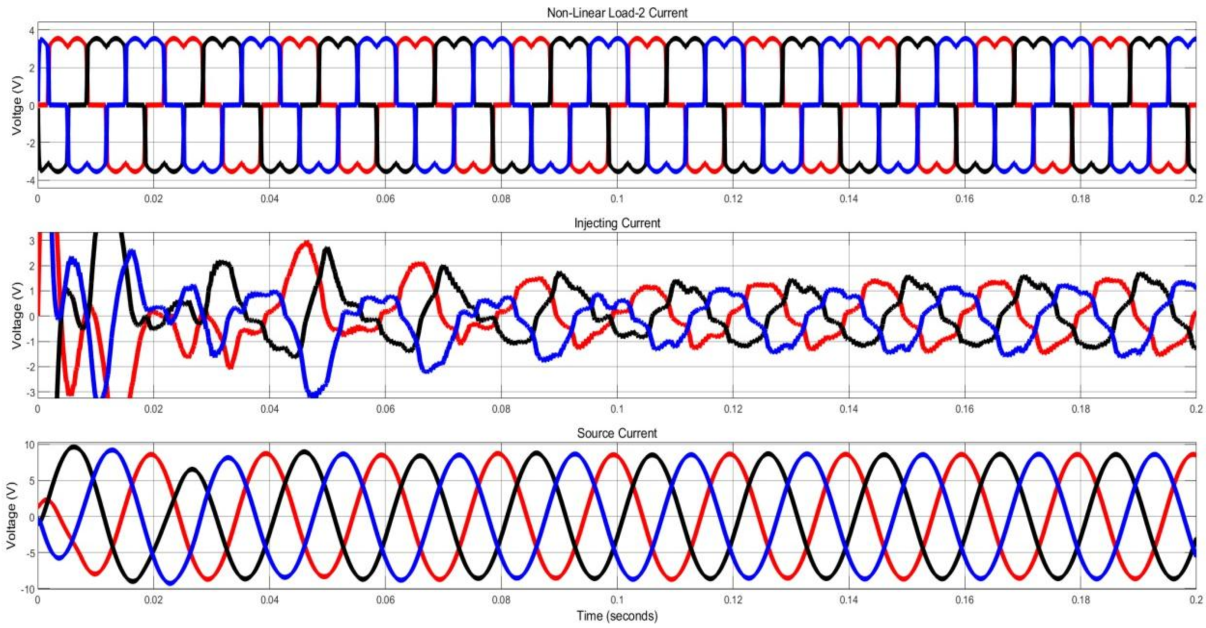

Figure 5: Non-linear load-2, Injecting and Source currents

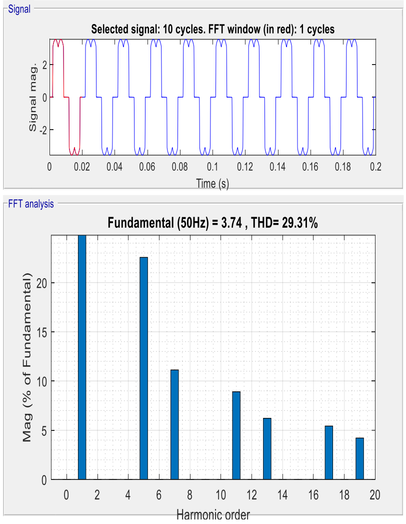

Figure 6a: Load current

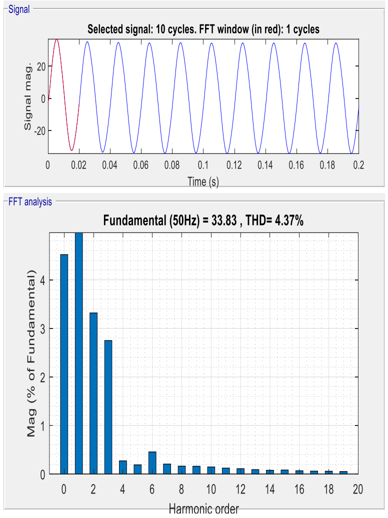

Figure 6b: Source current (PI)

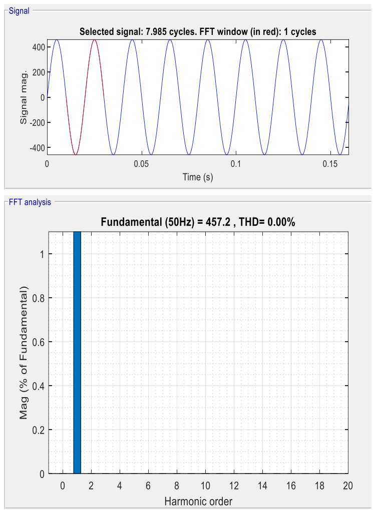

Figure 6c: Source current (ANN)

b. Voltage Harmonics injected at the Source

The performance of UPQC series compensators in microgrids is evaluated in terms of supply voltage distortion mitigation. The supply voltage is intentionally distorted with 30% third harmonic and 20% fifth harmonic components. Figure 7 displays the three-phase supply, compensation, and load voltages. At t = 0.02 sec, the series compensator is enabled, and the load voltage waveform at bus-2 approaches sinusoidality (Figure 9b). The load voltage's Total Harmonic Distortion (THD) drops dramatically from 36.06% to 0.0% after DVR correction (Figures 9a and 9b). This highlights the UPQC's ability to reduce THD and improve power quality.). Figure 8 depicts the relevant active and reactive power flows at gird, PCC, microgrid and load under these conditions.

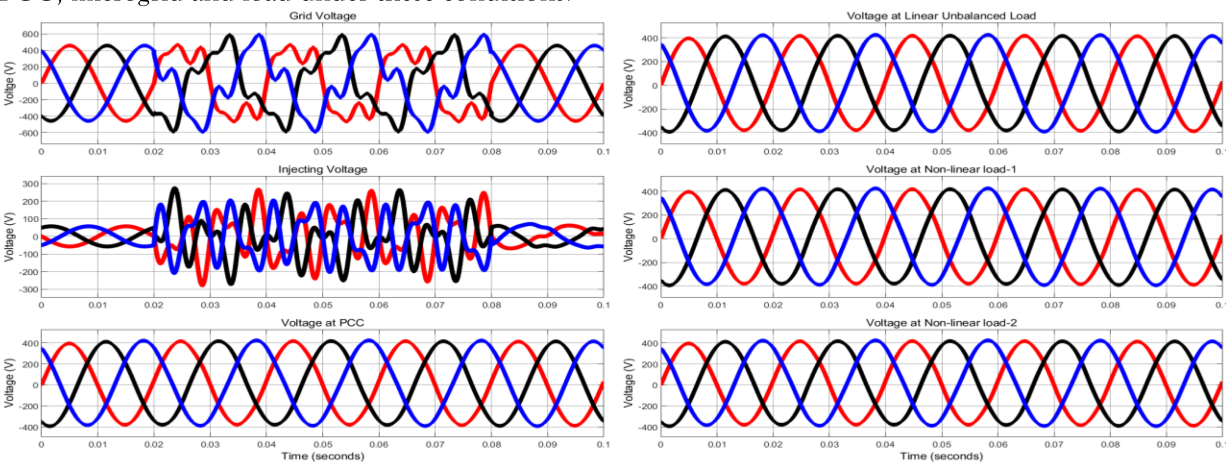

Figure-7: Grid, Injecting, Voltage at Non-linear load -1 and load-2

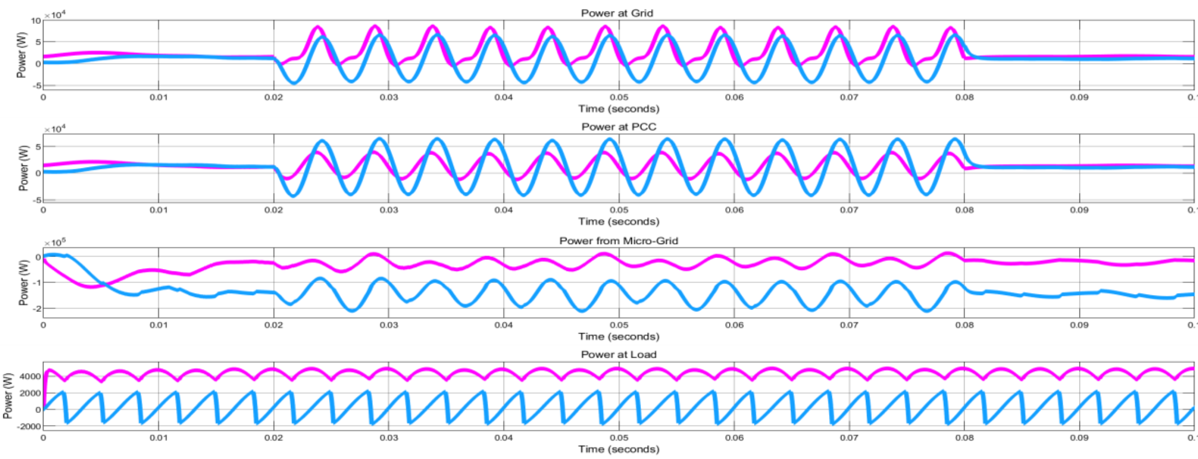

Figure 8: Powers at Grid, PCC, Micro-grid and Load

ISSN: 2229-7359
Vol. 11 No. 23s, 2025
https://theaspd.com/index.php

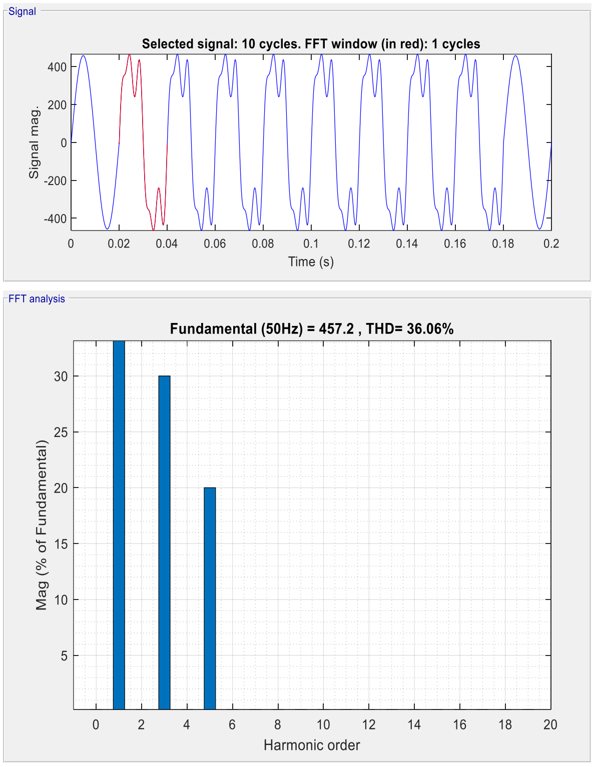

Figure 9a: THD of Grid Voltage

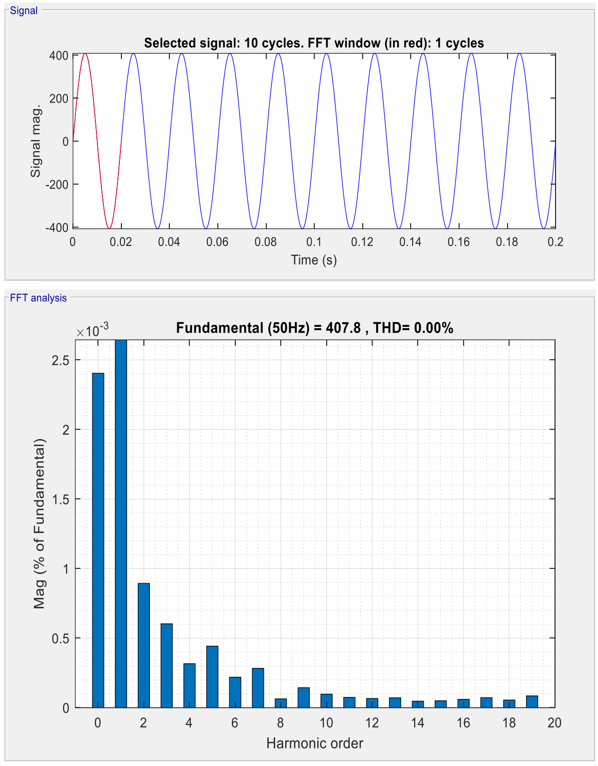

Figure 9b: THD of Load-1 Voltage

c. Voltage Sag at the Grid

Figure 12 shows that in this circumstance, the supply voltage sags by 0.3 p. u between 0.02 and 0.08 seconds (Figure 10a). The DVR recognizes the sag immediately and injects compensating voltages, as shown in Figure 10(b), to keep the load voltages at the correct level with minimal distortion, as shown in Figures 10(c) and 10(d), 10(e) and 10(f). Figure 11 depicts the relevant active and reactive power flows at gird, PCC, microgrid and load under these conditions.

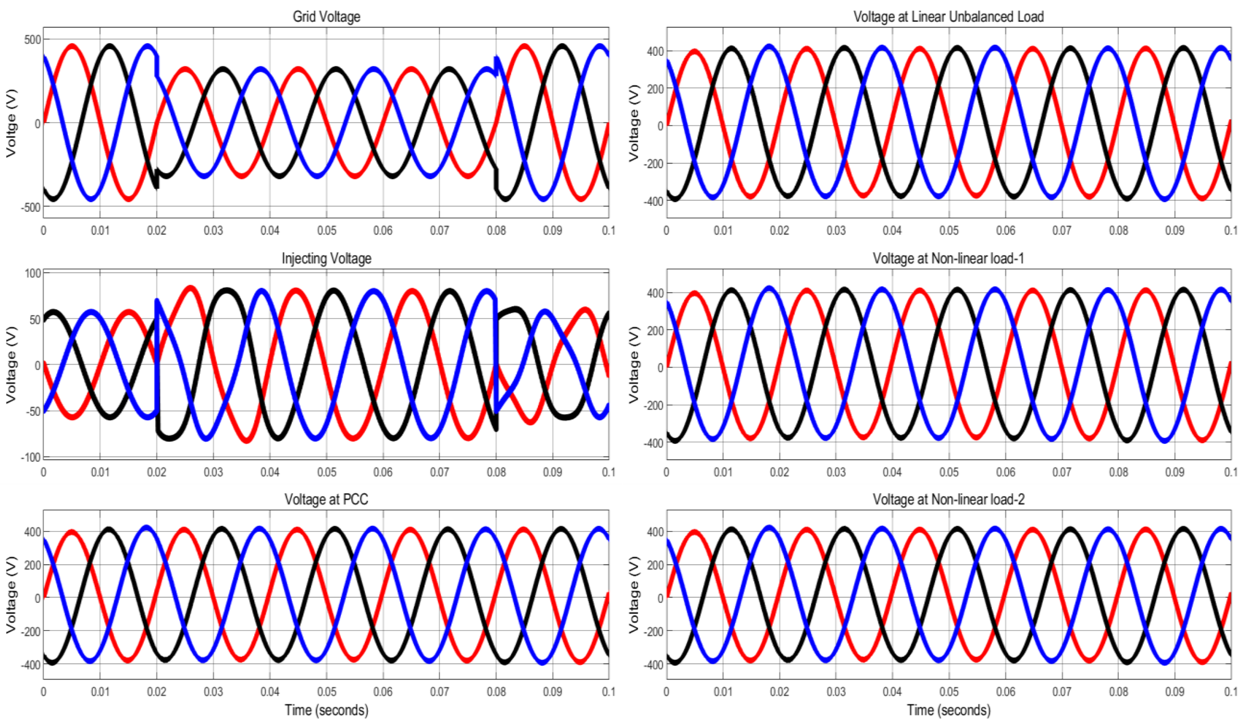

Figure 10: Voltage at Grid, Injecting, linear and Non-linear loads

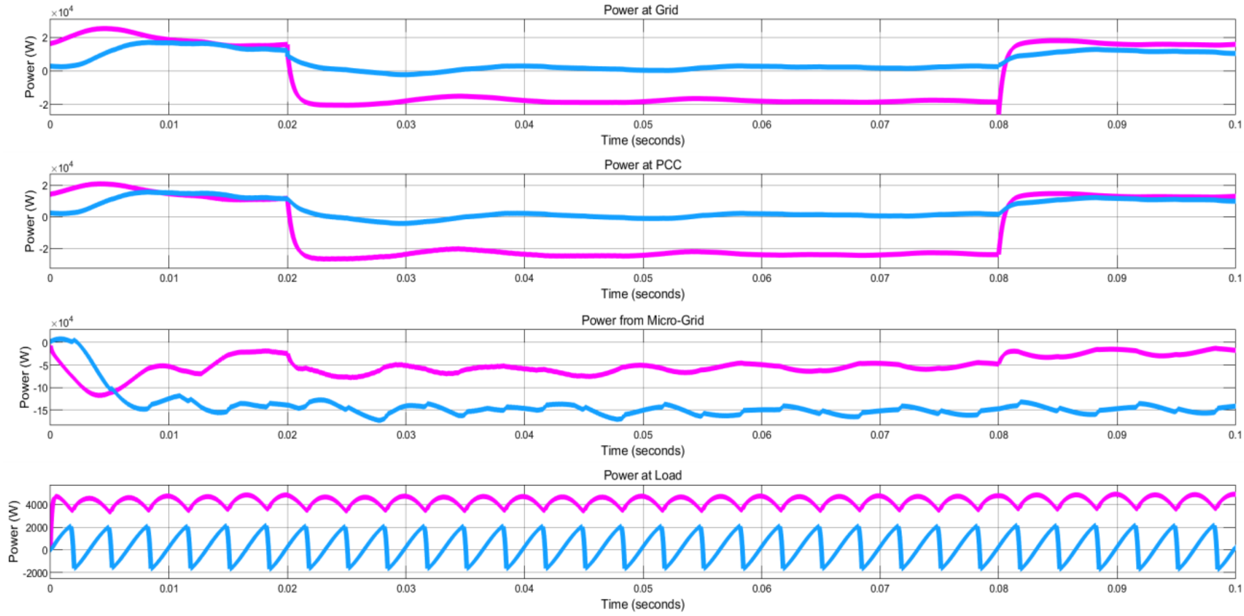

Figure 11: Powers at Grid, PCC, Micro-grid and Load

d. Voltage Swell at the Grid

When a voltage a rise of 0.3 p.u occurs between t = 0.02 sec and t = 0.08 sec (Figure 12a), the DVR recognizes the problem quickly and applies the correct mitigation voltages (Figure 12b). As a result, the load-2 voltage is efficiently controlled to the appropriate level, and harmonic components are removed, yielding a nearly sinusoidal waveform at PCC, linear unbalanced, Non-linear load-1 and load-2 are shown (Figure 12c, 12d, 12e and 12f). Figure 13 depicts the relevant active and reactive power flows at gird, PCC, microgrid and load under these conditions.

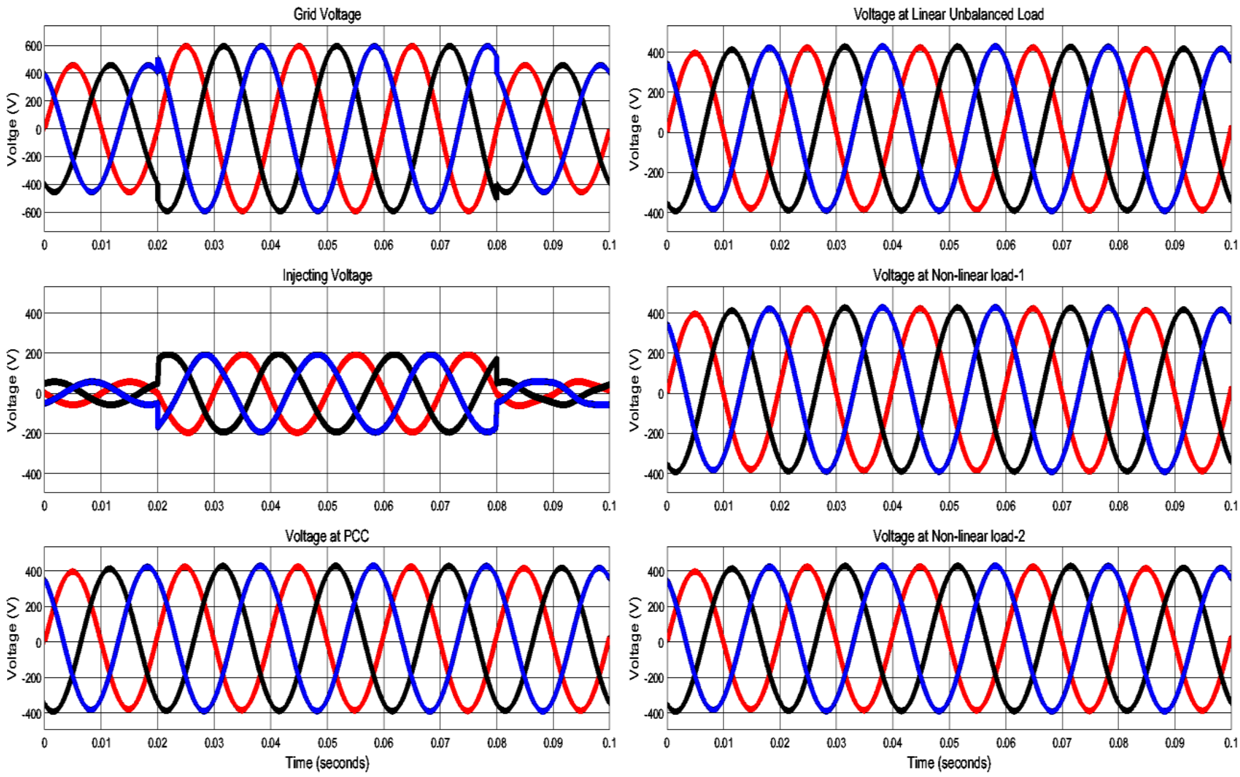

Figure 12: Voltage at Grid, Injecting, linear and Non-linear loads

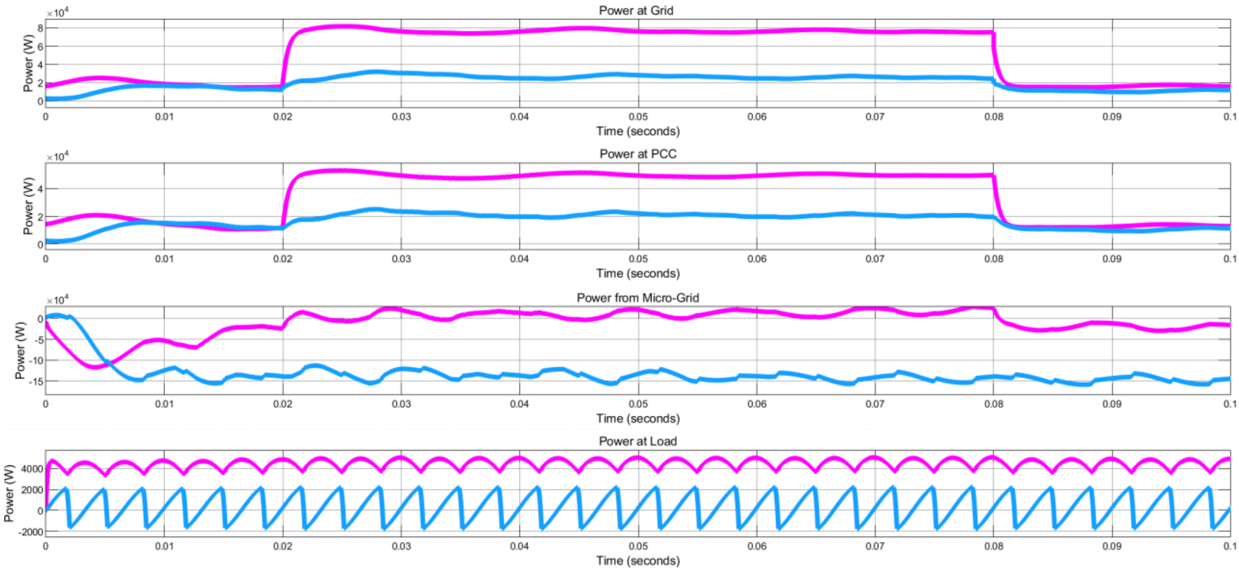

Figure 13: Powers at Grid, PCC, Micro-grid and Load

f. Interconnected and Island Mode - Timeline of the operating conditions

The positions of the switch (for open-0 and close-1) and the operation in both interconnected and islanded modes are studied from 0 to 0.5 seconds based on the integration method and signal generation for islanding detection and the reconnection method. Switches S1, S2, and S3 function in closed conditions while S4 operates in open conditions when under interconnected or normal settings. In island mode, these states are reversed. Normal operation lasts for 0.1 seconds at first, followed by 0.1 seconds of voltage sag, 0.1 seconds of islanding mode, 0.1 seconds of voltage swell and finally, at 0.4 seconds, the system is linked to the grid. Figure 14 illustrates each of these working situations.

Table 7 displays the operation schedules. During Islanding, the DVR is completely isolated with system and necessary power for loads is supplied through microgrid system. But during voltage sag and swell, DVR injects necessary voltage component to maintain voltage at rated level. Figure 15 demonstrates the corresponding active and reactive power flows under this condition at the grid, PCC, microgrid, and load.

Table 7: Different Operating Conditions

Operating Conditions	**Time in seconds**
Normal	0.0-0.1
Sag	0.1-0.2
Islanding	0.2-0.3
Swell	0.3-0.4
Reconnection	0.4-0.5

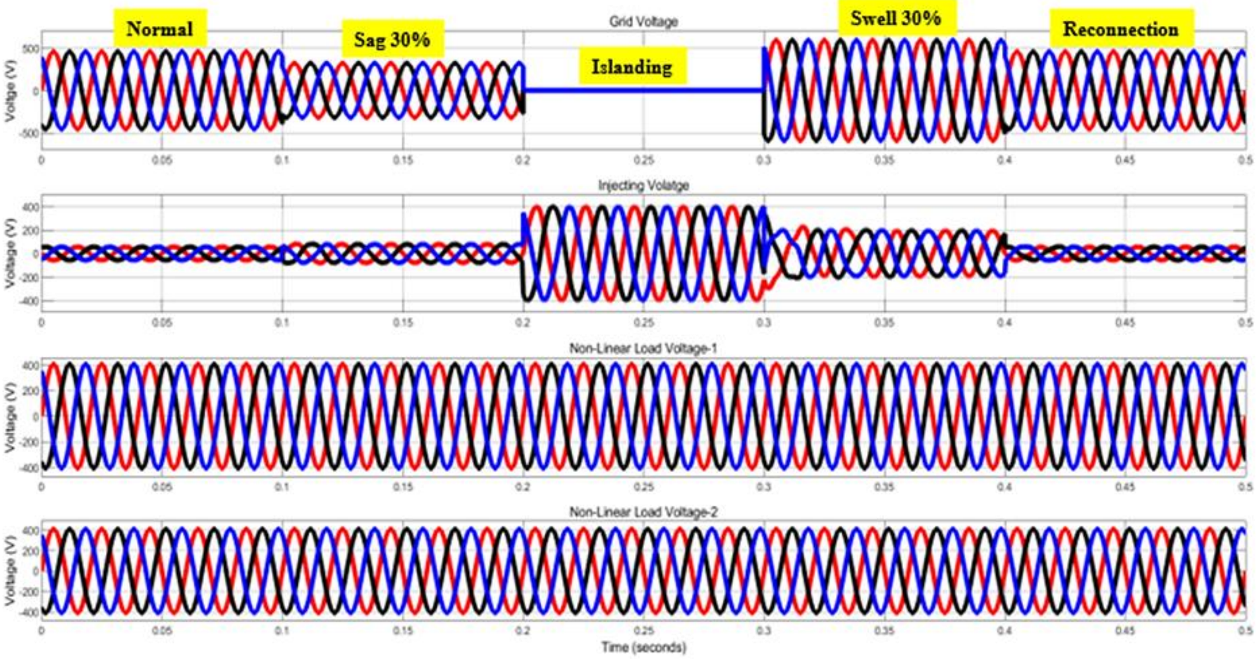

Figure 14: Voltage at Grid, Injecting and Non-linear loads

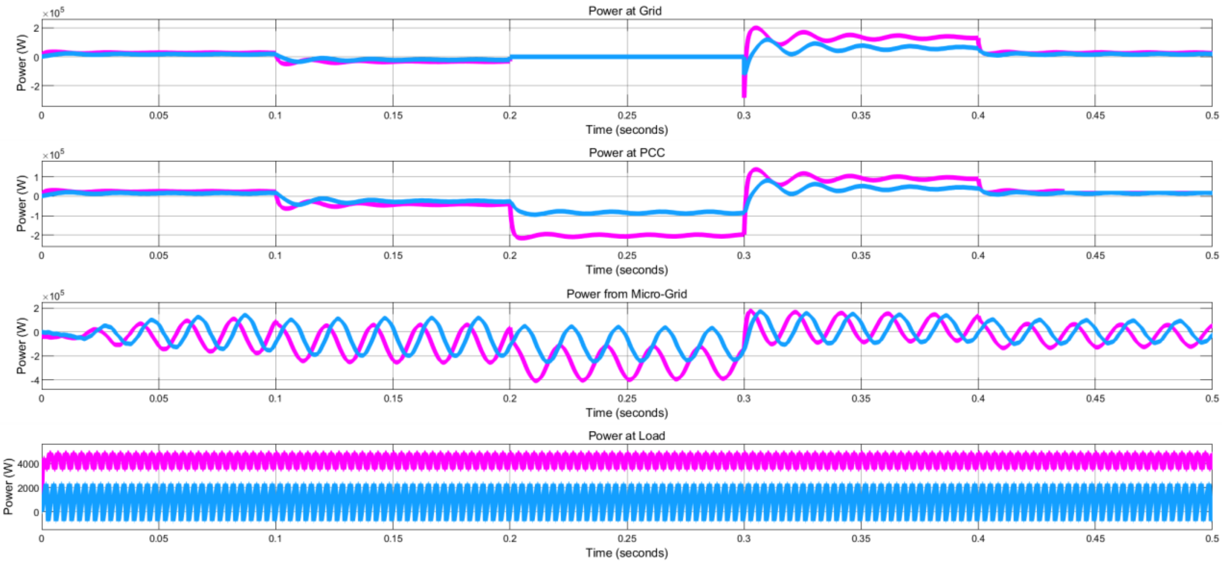

Figure 15: Powers at Grid, PCC, Micro-grid and Load

8. CONCLUSIONS

The implementation of a neural network-based control system for a Multi-Terminal Unified Power Quality Conditioner (MT-UPQC) has demonstrated significant potential in enhancing Electric Power Quality (EPQ) and stability within a microgrid environment. By leveraging the adaptive learning capabilities of neural networks, the proposed system effectively compensates for voltage sags/swells, harmonics, and reactive power disturbances, ensuring a more stable and reliable power supply. The control strategy dynamically adjusts to fluctuating load conditions and distributed energy sources, making it highly suitable for the complex and nonlinear behaviour typical of microgrids. Simulation results validate that the ANN-based controller outperforms traditional PI and heuristic controllers in terms of response time, accuracy, and robustness under various fault and load change scenarios.

Furthermore, the integration of the Levenberg–Marquardt training algorithm enabled fast convergence and precise function approximation, leading to optimal real-time control of the MT-UPQC. The improved voltage regulation, harmonic suppression in terms of maintaining THD of voltage and current harmonics with IEEE 519 standard and power factor correction contribute significantly to maintaining power quality standards and ensuring operational stability across the microgrid. In conclusion, the proposed ANN-based MT-UPQC control framework not only meets the demanding requirements of modern microgrids but also offers a scalable and intelligent solution to power quality management in distributed energy systems.

REFERENCES:

[1] DC- microgrid of smart university. IEEE Access (2021), https://doi.org/10.1109/ACCESS.2021.3095973

[2] P. Gajewski, Turbine, “photovoltaic panels and battery energy storage,” Energies 14(6), 1595 (2021)
[3] B. Priyadharshini, V. Ganapathy, P. Sudhakara, “An optimal modelto meet the hourly peak demands of a specific region with solar, wind, and grid supplies,” IEEE Access 8, 13179–13194 (2020). https://doi.org/10.1109/ACCESS.2020.2966021
[4] K. Sarita et al., “Power enhancement with grid stabilization of renewable energy-based generation system using UPQC-FLC- EVA technique,” IEEE Access 8, 207443–207464 (2020). https://doi.org/10.1109/ACCESS.2020.3038313
[5] D. Kolantla, S. Mikkili, S.R. Pendem, A.A. Desai, “Critical reviewon various inverter topologies for PV system architectures,” IET Renew. Power Gener. 14(17), 3418–3438 (2020). https:// doi.org/10.1049/iet-rpg.2020.0317
[6] R. Li, F. Shi, “Control and optimization of residential photovoltaicpower generation system with high efficiency isolated bidirectional dc-dc converter,” IEEE Access 7, 116107–116122 (2019).
[7] A.C. Luna, N.L. Diaz, M. Graells, J.C. Vasquez, J.M. Guerrero, “Mixed-integer-linear-programming-based energy management system for hybrid PV-wind-battery microgrids: modeling, design, and experimental verification,” IEEE Trans. Power Electron. 32(4),2769–2783 (2017).
[8] S.D. Al-Majidi, M.F. Abbod, H.S. Al-Raweshidy, “A particleswarm optimization-trained feedforward neural network for pre- dicting the maximum power point of a photovoltaic array,” Eng. Appl. Artif. Intell.Artif. Intell. (2020). https://doi.org/10.1016/j. engappai.2020.103688
[9] R.B. Roy et al., “A comparative performance analysis of ANN algorithms for MPPT energy harvesting in solar PV system,” IEEE Access 9, 102137–102152 (2021).
[10] A.T. Peiris, J. Jayasinghe, U. Rathnayake, “Forecasting wind powergeneration using artificial neural network: ‘Pawan danawi’-A casestudy from Sri Lanka,” J. Electric. Comput. Eng. (2021). https:// doi.org/10.1155/2021/5577547
[11] K. Prabaakaran, R. Srividhya, R.S. Kumar, D.H. Kumar, D.M. Raj, A.S. Prabu, “Energy Management system for small-scale hybrid wind solar battery-based microgrid,” EAI/Springer Innov. Commun. Comput. 8, 493–501 (2022). https://doi.org/10.1007/ 978-3-030-86165-0_42
[12] M.M. Gulzar, A. Iqbal, D. Sibtain, M. Khalid, “an innovative converter less solar PV control strategy for a grid connected hybrid PV/Wind/fuel-cell system coupled with battery energy storage,” IEEE Access 11(March), 23245–23259 (2023). https://doi.org/ 10.1109/ACCESS.2023.3252891
[13] A.A.M. Nureddin, J. Rahebi, A. Ab-Belkhair, “Power managementcontroller for Microgrid integration of hybrid PV/fuel cell systembased on artificial deep neural network,” Int. J. Photo energy Photo energy (2020). https://doi.org/10.1155/2020/8896412
[14] P. Roy, J. He, T. Zhao, Y.V. Singh, “Recent Advances of wind-solarhybrid renewable energy systems for power generation: a review,” IEEE Open J. Indus. Electron. Soc. 2022. https://doi.org/10. 1109/OJIES.2022.3144093
[15] A. Tuckey, S. Round, “Grid-Forming inverters for grid-connected Microgrids,” IEEE Electrif. Magaz. 10(1), 39–51, 2022
[16] F.M.A. Hadi, H.H. Aly, T. Little, “Harmonic forecasting of wind and solar hybrid model driven by DFIG and PMSG using ANN and ANFIS,” IEEE Access (2023). https://doi.org/10.1109/ ACCESS.2023.3253047
[17] A.M. Jasim, B.H. Jasim, V. Bures, P. Mikulecky, “A novel co-operative control technique for hybrid AC/DC smart Microgrid converters,” IEEE Access **11**(January), 2164–2181 (2023). https://doi.org/ 10.1109/access.2023.3234011
[18] Saini, K., Saini, M., Kumar, A. et al. Performance analysis and optimization in renewable energy systems: a bibliometric review. Discov. Appl. Sci. 7, 178 (2025). https://doi.org/10.1007/s42452-025-06585-2.
[19] P. Chandra Babu et al., “Modeling and Performance Analysis of a Grid-Connected Photovoltaic System with Advanced Controller considering Varying Environmental Conditions,” Int. J. Energy Res., 2023.
[20] Aslam, M.U, Shakhawat, Shah R Amjady, N, Miah, M.S Amin, B.M.R, “Hybrid Energy Storage Modeling and Control for Power System Operation Studies: A Survey” Energies 2024, 17, 5976. https://doi.org/10.3390/en17235976.
[21] Szpilko, Danuta, Xavier Fernando, Elvira Nica, Klaudia Budna et al "Energy in Smart Cities: Technological Trends and Prospects." MDPI 17, no. 24, 2024, 6439.
[22] Bade, S. O., Tomomewo, O. S., Meenakshisundaram, A., Dey, M., Alamooti, M., & Halwany, N. (2025). Multi-Criteria Optimization of a Hybrid Renewable Energy System Using Particle Swarm Optimization for Optimal Sizing and Performance Evaluation. Clean Technologies, 7(1), 23. https://doi.org/10.3390/cleantechnol7010023
[23] Szpilko D, Fernando X, Nica E, Budna K, Rzepka A, Lăzăroiu G. Energy in Smart Cities: Technological Trends and Prospects. Energies. 2024; 17(24):6439. https://doi.org/10.3390/en17246439
[24] P. Kundur, “Power System Stability and Control,” McGraw-Hill, 1994.
[25] R. Yadav, B. Singh, and D. T. Shahani, “ANN-based control of solar PV and wind hybrid system with battery storage,” IEEE Transactions on Industrial Applications, vol. 54, no. 1, pp. 17–26, 2018.
[26] S. Chapala, N. R.L., T. R. D. G and G. S. Lakshmi, "PV and Wind Distributed Generation System Power Quality Improvement Based on Modular UPQC," 2023 International Conference on Advanced & Global Engineering Challenges (AGEC), Surampalem, Kakinada, India, 2023, pp. 82-87, doi: 10.1109/AGEC57922.2023.00027.
[27] B. Pattanayak, S. Nanda and N. Kumar, "Application of UPQC in Enhancing Power Quality of Microgrid Linked to PV, Wind & Battery with ANN MPPT," 2024 3rd Odisha International Conference on Electrical Power Engineering, Communication and Computing Technology (ODICON), Bhubaneswar, India, 2024, pp. 1-6, doi: 10.1109/ODICON62106.2024.10797487.
[28] P. Ray, P. K. Ray, P. S. Puhan and M. L. T. K. Liyanage, "Performance Improvement of Microgrid with Strategic Control of Distributed Energy Resources Integrated UPQC," in IEEE Transactions on Industry Applications, vol. 61, no. 3, pp. 4695-4705, May-June 2025, doi: 10.1109/TIA.2025.3539616.

BIOGRAPHIES:

Manjula M G was born in Karnataka, India in 1985. She received the B.E and Master’s degrees from the Visveswaraya Technological University, Belgavi, Karnataka, in 2006 and 2009. Currently, she is pursuing Ph.D degree in the field power quality and working as Assistant professor in the Department of Electrical Engineering, JNN College of Engineering, Shimoga, Karnataka. Her research interests include Power System, Microgrid, Power Electronics and Power Quality.

Dr. Surendra S was born in Karnataka, India in 1968. He received the B.E degree from Mysore University and Master’s degree from Mangalore University in Industrial electronics, Karnataka, in 1989 & 1992 and Ph.D degree from IISc, Bangalore in 2012. Currently he is working as professor & HOD in the Department of Electrical Engineering, JNN College of Engineering, Shimoga, Karnataka. His research interests include Power System, Power Electronics and Power Quality.